Microchimica Acta (2019) 186: 498
https://doi.org/10.1007/s00604-019-3613-4

ORIGINAL PAPER

A dual (colorimetric and fluorometric) detection scheme for glutathione and silver (I) based on the oxidase mimicking activity of MnO_2 nanosheets

Zhangyan Ma[1] · Tengteng Wu[1] · Peipei Li[1] · Meiling Liu[1] · Si Huang[1] · Haitao Li[1] · Youyu Zhang[1] · Shouzhuo Yao[1]

Received: 27 February 2019 / Accepted: 14 June 2019 / Published online: 3 July 2019

Abstract
A fluorimetric and colorimetric method is described for the determination of glutathione (GSH) and silver (I). It is based on the use of MnO_2 nanosheets that were prepared by solution mixing and exfoliation. They display oxidase-mimicking activity and can catalyze the oxidation of o-phenylenediamine (OPD) to form yellow 2,3-diaminophenazine (DAP) with an absorption maximum at 410 nm. DAP also has a yellow fluorescence (with a peak at 560 nm). The MnO_2 nanosheets can be rapidly reduced to Mn^{2+} by GSH. This reduces the efficiency of the oxidase mimic MnO_2 and causes a decrease in fluorescence and absorbance intensity. However, on addition of Ag^+, a complex is formed with GSH. It prevents the destruction of MnO_2 nanosheets so that the enzyme mimicking activity is retained. A dual-method for the determination of GSH and Ag(I) was developed. It has excellent sensitivity for GSH with lower detection limits of 62 nM (fluorimetric) and 0.94 μM (colorimetric). The respective data for Ag(I) are 70 nM and 1.15 μM. The assay was successfully applied to the determination of GSH and Ag(I) in spiked serum samples.

Keywords MnO_2 nanosheets · Dual-readout · Dual-component · Colorimetric and fluorometric method · GSH and Ag^+

Introduction

The concentration of some life-related small molecules is closely related to disease issues [1, 2]. Therefore, qualitative and quantitative detection can help to provide valuable information for human health [3]. However, owing to the diversity of diseases and the complexity of biological samples, it is still a great challenge to the precise analysis. Therefore, it is necessary to develop more reliable method. The simultaneously detection of two or multiple components is attractive owing to their convenience for realization of multiple purposes [4]. For example, the continuous detection of the copper(II) ion and cysteine (Cys) [5], mercury(II) and Cys [6] have been reported based on the fluorescent nanoprobes. The sensing assays with multiple signals is more selective and sensitive [7]. For example, fluorometric/magnetic bimodal sensor used for the detections of H_2O_2 [8], fluorometric and colorimetric dual-readout for mercury(II) have been reported [9]. Thus, there is considerable interest in developing multi-components detection with multiple signals via the usage of novel functional materials, which can get comprehensive and reliable information.

The rapid development of nanomaterials has brought great opportunities and progress in disease-related fields [10, 11]. Two dimensional nanosheets or nanoflakes have attracted much attention owing to their larger surface area, unique optical features, oxidase or peroxidase mimicking activity [12, 13]. Cobalt oxyhydroxide nanoflakes-carbon dots can monitor ascorbic acid in rat brain [14] and Ti_3C_2 MXenes can detect exosomes in cells [13] based on the fluorescence resonance energy transfer (FRET). V_2O_5 nanosheets with oxidase-like activity can detect glutathione (GSH) in human serum samples [15]. Among the two-

Electronic supplementary material The online version of this article (https://doi.org/10.1007/s00604-019-3613-4) contains supplementary material, which is available to authorized users.

✉ Meiling Liu
liumeilingww@126.com; liuml@hunnu.edu.cn

[1] Key Laboratory of Chemical Biology & Traditional Chinese Medicine Research (Ministry of Education, China), College of Chemistry and Chemical Engineering, Hunan Normal University, Changsha 410081, People's Republic of China

dimensional nanosheets, MnO_2 has attracted intense attention because the fascinating characteristics, such as surface property, wide absorption peak, redox properties and biological compatibility [16, 17]. MnO_2-fluorescent polydopamine nanoparticles was applied for alkaline phosphatase (ALP) detection in human serum samples [18], MnO_2-AuNCs can be used for the detection of H_2O_2 based on FRET [8], MnO_2 NFs with tandem enzyme-like activities (GOx-like activity and peroxidase-like activity) can realize the rapid qualitative analysis of glucose by spectrophotometry or visually [19], MnO_2-modified UCNPs can rapidly screen and quantify GSH in cancer cells [20]. To this end, developing MnO_2 based nanoplatform with dual-readouts for multiple components in complex samples is a promising work.

GSH is one of the most typical small molecules, its imbalance is closely associated with numerous clinical diseases, such as cancer, Alzheimer's disease, liver disease, HIV, heart attack and other ailments [21, 22]. Silver ions (Ag^+) is one of the hazardous metal ions, which is also highly related to health owing to their bioaccumulation characteristics and widely usage in various fields. Overused Ag^+ has brought about a series of problem in environment and health, such as suppressing sulfhydryl enzymes, silver poisoning and silver accumulation [23, 24]. Thus, it is necessary to develop simple and sensitive methods to detect GSH and Ag^+. A self-cascade catalytic system based on cupric oxide nanoparticles (CuO NPs) was designed for GSH and Ag^+ ions [25] via intrinsic GSH-oxidase and peroxidase-like activity of CuO NPs. It is effective for detection of GSH and Ag^+ in serum and tap water, respectively. However, only single channel was utilized, and it is difficult to realize the simultaneously or continuously detection. Thus, it is necessary to develop a simple method with multiple signals, which can be used in the same complex sample for multi-components.

In this work, MnO_2 nanosheets with enzymatic-like activity were prepared and used as the dual-readout nanoprobe for the detection of GSH and Ag^+ sensitively. As illustrated in Scheme 1, MnO_2 nanosheets can oxidize OPD to DAP with the change of fluorescence and colorimetric signals. GSH can destroy the structure of MnO_2 nanosheets and affect the enzymatic-like property of the MnO_2, which will result in decrease of fluorescence and absorbance intensity of the system. However, when Ag^+ is added, it can form a complex with GSH [26] and prevent the destruction of MnO_2 nanosheets. Interestingly, the Ag^+ also can oxidize OPD to DAP [27], to this end, the detection of Ag^+ via response of fluorescence and absorbance of the system can be realized with increased sensitivity compared with that without GSH. The detection mechanism is thoroughly investigated using various experiments. And it proved that the detection is based on the change of the enzymatic-like properties of MnO_2 nanosheets owing to the damage-protection strategy. The method based on MnO_2-OPD is a dual-readout detection platform for GSH and Ag^+, which provided more reliable and comprehensive information. The method can detect different components in the same complex sample, which is more convenient and practical. These demonstrate their potential applications in clinical diagnosis and treatment.

Experimental section

Reagents and materials

The single-layer manganese dioxide nanosheets were prepared as literature with slight modification [1]. Tetramethylammonium hydroxide (TMA·OH, 25%) were obtained from Tianjin Guangfu Fine Chemical Research Institute (Tianjin, China, http://www.guangfu-chem.com/), o-phenylenediamine (OPD, 99.0%), manganese chloride tetrahydrate ($MnCl_2·4H_2O$, 99.0%) were purchased from Tianjin Commio Chemical Testing Co., Ltd. (Tianjin, China, http://www.chemreagent.com/), hydrogen peroxide (H_2O_2, 30 wt%) were provided from Shanghai Wokai Biotechnology Co., Ltd. (Shanghai, China, https://ml.hgxqp.com/), L-glutathione reduced (GSH, 98.0%) were purchased from Aladdin industrial corporation (Shanghai, China, https://www.aldjf.com/), bovine serum albumin (BSA, 98.0%) were obtained from Sigma-Aldrich (https://www.sigmaaldrich.com/), di-potassium hydrogen phosphate (K_2HPO_4, 99.5%), potassium dihydrogen phosphate (KH_2PO_4, 99.5%) and silver nitrate ($AgNO_3$,99.8%) were purchased from Sinopharm chemical reagent Co., Ltd. (Shanghai, China, https://www.reagent.com.cn/). All other chemicals were of analytical grades and used without further purification. Ultrapure water was purified using a Milli-Q system.

Apparatus

Fluorescence spectrometer F-7000 (Hitachi, Japan) was applied for FL analysis. UV–vis spectra were obtained from UV-2450 (Shimadzu, Japan). Fourier infrared spectra (FTIR) were recorded on Nexus-870 (Thermo Nicolet, USA). Energy dispersive spectrometer (EDS) and morphology images of MnO_2 nanosheets were obtained on a transmission electron microscope (TEM) JEM-2100 (JEOL, Japan). X-ray photoelectron spectroscopy (XPS) were obtained from K-Alpha 1063 (Thermo Fisher Scientific, British). X-ray diffraction (XRD) patterns were collected using a Rigaku 2500 (Japan) X-ray diffractometer.

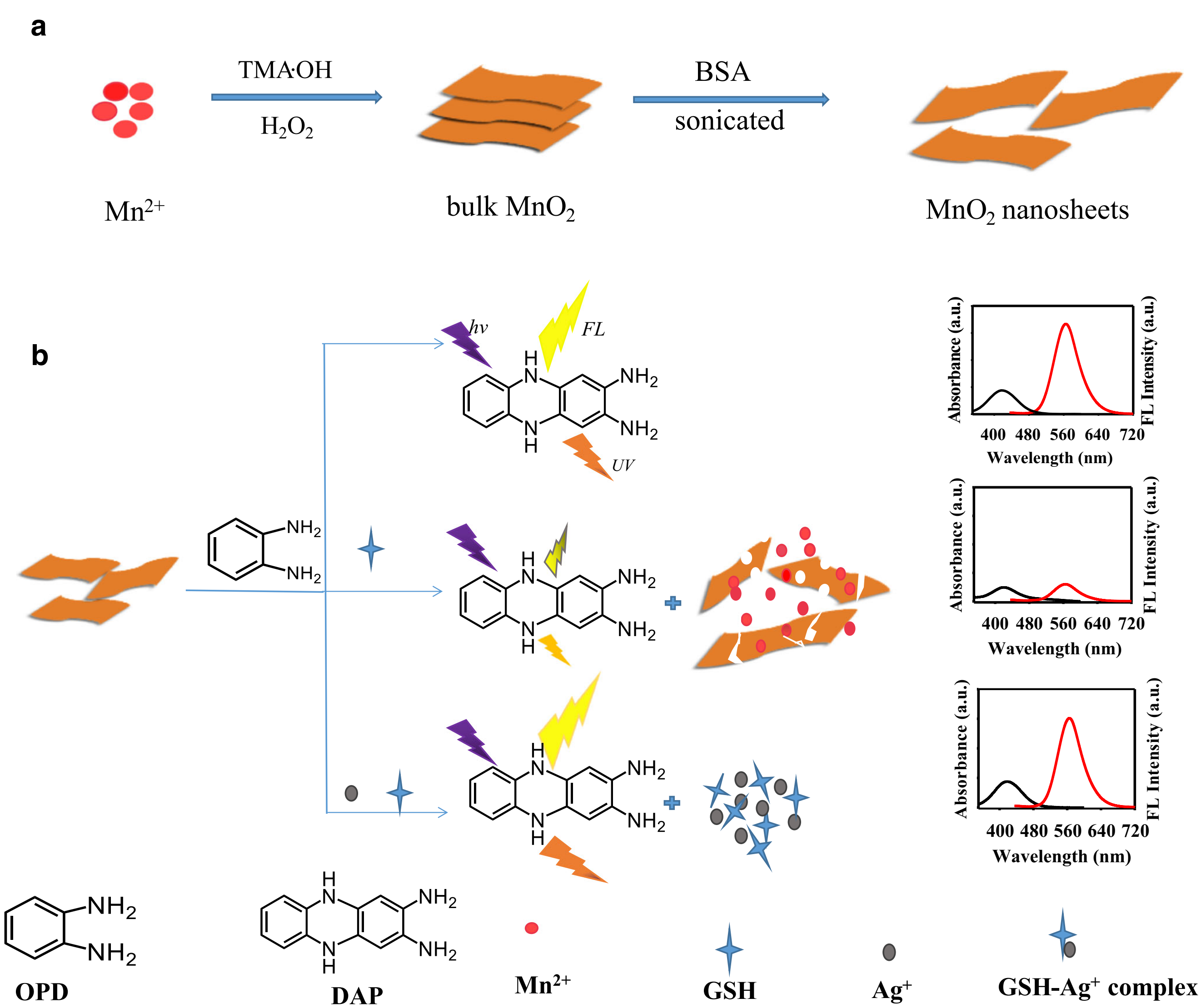

Scheme 1 Schematic presentation of the synthesis of MnO_2 nanosheets (**a**) and the schematic illustration of fluorometric and colorimetric detection of GSH and Ag^+ on the basis of MnO_2-OPD (**b**)

Colorimetric and fluorometric assay of GSH and Ag^+

A stock solution of GSH (100 mM) was prepared in water and various concentrations of GSH were obtained by serial dilution of the stock solution. For the detection of GSH, 100 μL of GSH solution at different concentrations were added sequentially to 600 μL of 0.1 M PBS (pH 7.0) and 100 μL of MnO_2 nanosheets aqueous solution (200 μM), then 100 μL of 3 mM OPD was added, the total volume of the reaction solution was 1.0 mL. After that, the solution was mixed thoroughly and incubated for 40 min at 60 °C. Finally, colorimetric and fluorescence detection were performed.

The method of detecting Ag^+ is similar to detecting of GSH. First, 100 μL of 100 μM GSH solution was mixed with different concentration of Ag^+ (100 μL). Then, the mixed solution was added to 600 μL of 0.1 M PBS (pH 7.0) and 100 μL of MnO_2 nanosheets aqueous solution (200 μM), then added 100 μL of 3 mM OPD, and the total volume of the reaction solution was 1.0 mL. After that, the mixture was mixed thoroughly and incubated for 40 min at 60 °C. Finally, colorimetric and fluorescence detection were performed.

Selectivity

To elevate the selectivity of the method, interferences including common metal ions (Na^+, Ca^{2+}, Mn^{2+}, Mg^{2+}, Al^{3+}, Hg^{2+}, Cd^{2+}, Cr^{3+}, Pb^{2+}), amino acids including glycine (Gly), glutamine (Gln), histidine (His), lysine (Lys), glutamic acid (Glu), tyrosine (Tyr), serine (Ser), alanine (Ala), cysteine (Cys), and other biological compounds like ascorbic acid (AA) that usually coexisted with GSH and Ag^+ were studied under fluorescence and colorimetric modes.

Detection of GSH and Ag^+ in real samples

Human serum samples (provided by the Hospital of Hunan Normal University) were treated by centrifugation for 10 min, filtered through a 0.22 μm microporous membrane, and immediately diluted 100 times. Tap water and River water were obtained from our laboratory and the Xiangjiang river located in Changsha, Hunan province, respectively. The water samples were filtered through a 0.22 μm membrane and then diluted 10 times. GSH and Ag^+ were detected as described above using the standard additional method.

Results and discussion

Characterization of MnO_2

MnO_2 nanosheets were characterized by TEM, UV-vis, FTIR, XRD, XPS and EDS. As illustrated in Fig. 1a, MnO_2 nanosheets exhibit a typical sheet structure with folds and crinkles. MnO_2 nanosheets have a wide absorption band at 300–800 nm with the absorption peak at 380 nm (Fig. 1b) and show dark brown color under sunlight (Fig. 1b, inset). As the FTIR spectra shown in Fig. 1c, MnO_2 nanosheets have characteristic peak at about 500 cm^{-1} attributed to the Mn-O stretching vibrations. The peaks around 1636 cm^{-1} may be attributed to O-H bending vibrations combined with Mn atoms, and the peak at 3415 cm^{-1} suggest the O-H bond stretching vibrations, which are consistent with previous literature [28]. In Fig. 1d, the XRD pattern shows four diffraction peaks located at about 18°, 26°, 36° and 65°, which are indexed as (002), (003), (100) and (110). These suggest the MnO_2 nanosheets has a layered structure as well [29]. In order to further prove the formation of MnO_2 nanosheets, XPS of typical product was recorded (Fig. 1e). The peak of 641.9 eV is fitted into $2p_{3/2}$ and the peaks of 642.4 eV, 641.9 eV and 640.9 eV are fitted into Mn^{4+}, Mn^{3+} and Mn^{2+}, respectively, which accords well with XPS patterns of MnO_2 [30, 31]. EDS in Fig. 1f suggests that the main element is Mn and O. Therefore, the above results confirm the formation of MnO_2 nanosheets.

Feasibility of detecting GSH and Ag^+

The intrinsic oxidase-like activity of MnO_2 nanosheets was verified. In Fig. S1, MnO_2 nanosheets can catalyze OPD, TMB and ABTS to yellow, blue and green oxidized product, respectively, showing that the MnO_2 nanosheets has oxidase-like activity. Using the typical oxidation of OPD as an example, MnO_2 nanosheets can catalyze the colorless OPD to yellow DAP [16] and lead to the fluorescence and colorimetric signal change. The dual-readout platform may be used for detection of some components that can change the oxidase-like property of MnO_2 nanosheets. Figure 2a, d suggest that the absorbance and fluorescence intensity reduce when GSH is added, but increase in the presence of Ag^+ for the system of MnO_2-OPD-GSH. As the concentration of GSH increase, the intensity decreases gradually (Fig. 2b, e), while the concentration of Ag^+ increase, the absorbance and fluorescence intensity enhance gradually (Fig. 2c, f). It is suggested that the

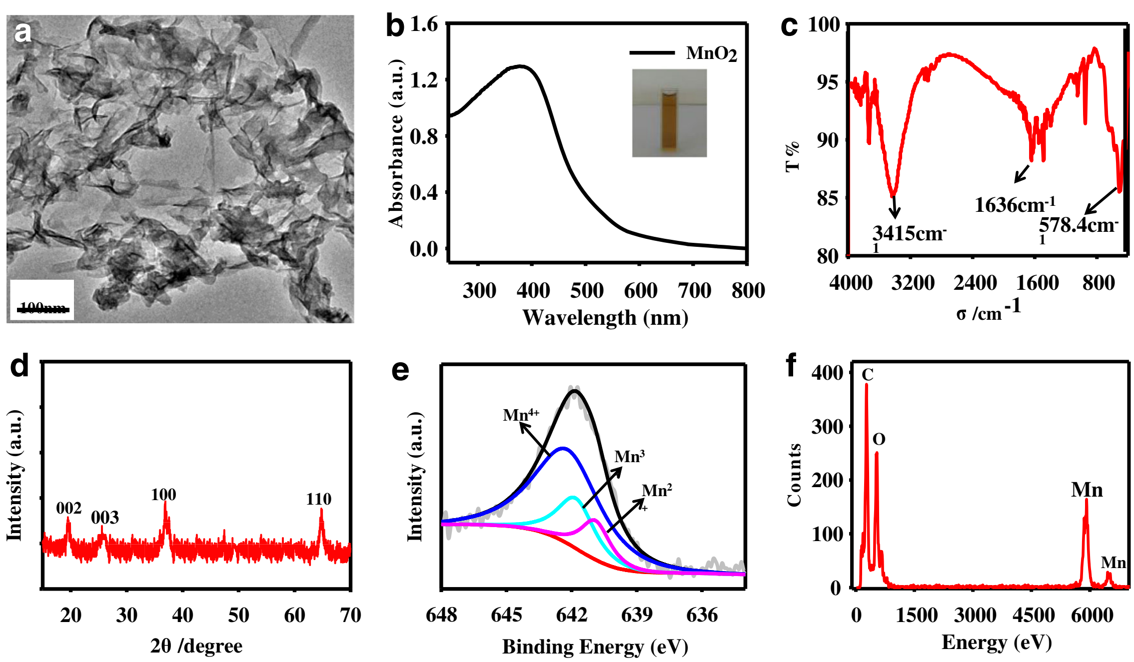

Fig. 1 **a** TEM image, **b** UV-vis spectra (inset shows the photographs of MnO_2 nanoflakes solution under visible light), **c** FT-IR spectra, **d** X-ray diffraction pattern, **e** XPS and **f** EDS of MnO_2 nanosheets

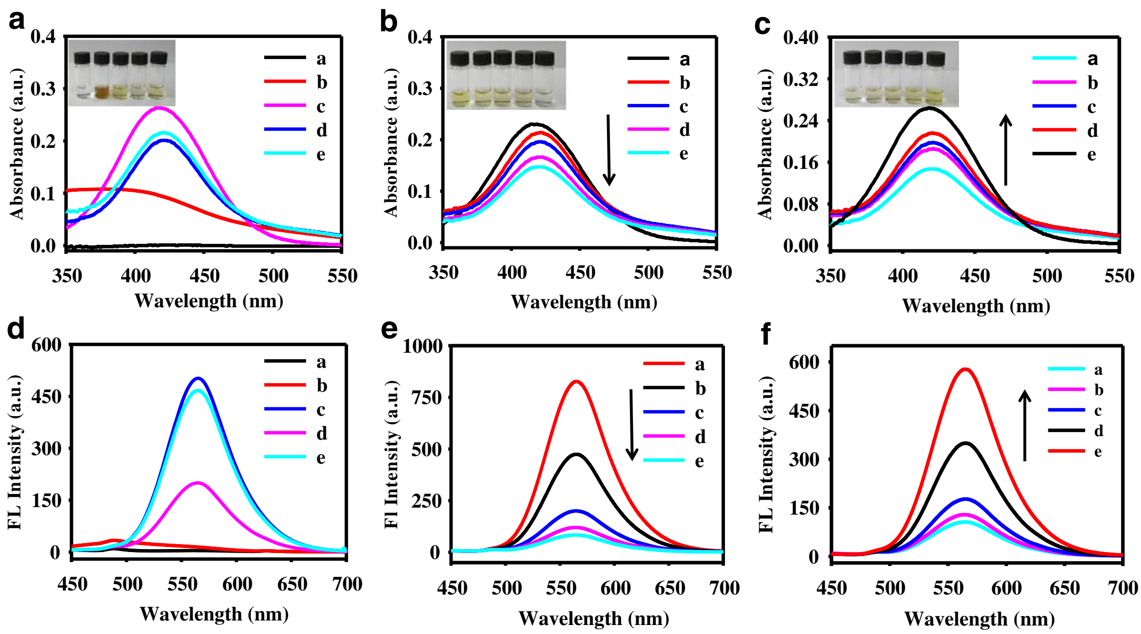

Fig. 2 **a** Absorbance of OPD (a), MnO_2 (b), MnO_2-OPD (c), MnO_2-OPD-GSH (d), OPD-MnO_2-GSH-Ag^+ (e). Changes in absorbance with different concentrations of GSH (**b**) and Ag^+ (**c**), inset shows the photographs of corresponding solution under visible light. **d** Fluorescence emission spectra of OPD (a), MnO_2 (b), OPD-MnO_2 (c), OPD-MnO_2-GSH (d), OPD-MnO_2-GSH-Ag^+ (e). The Changes in fluorescence with different concentrations GSH (**e**) and Ag^+ (**f**). Concentrations for GSH, 0.0 μM (a), 16.7 μM (b), 33.3 μM (c), 50.0 μM (d), 66.7 μM (e); Concentrations for Ag^+, 0.0 μM (a), 5.0 μM (b), 10.0 μM (c), 15.0 μM (d), 20.0 μM (e)

fluorescence and colorimetric signal change based on MnO_2-OPD can be used for testing of GSH and Ag^+ precisely.

Mechanism study

To investigate the mechanism of this platform, the TEM, UV-vis spectroscopy, fluorescence spectrum, and XPS were further investigated. As can be seen from the TEM (Fig. 3a), the nanosheets break into smaller nanosheets and Mn^{2+}, which is greatly different from the MnO_2 nanosheets. It indicates that the MnO_2 nanosheets may be damaged by GSH. In Fig. 3b, it can be seen that the absorbance intensity decreases, and the color of solution fades (inset of Fig. 3b) with the increasing of GSH concentration. It can be suspected that GSH can reduce the MnO_2 to Mn^{2+} as shown in Eq. (1).

$$MnO_2 + 2GSH + 2H^+ \rightarrow Mn^{2+} + GSSG + 2H_2O \qquad (1)$$

In Fig. 3c of XPS, the peak of Mn^{4+} on the Mn $2p_{3/2}$ spectrum decreases obviously and the peak of Mn^{2+} increases greatly after the addition of GSH compared with Fig. 1e, which reveals that MnO_2 is reduced to Mn^{2+} by GSH.

In Fig. 3d, e, when Ag^+ and MnO_2 incubated with OPD, respectively, the absorbance and fluorescence intensity are both enhanced. OPD was added to the mixed solution of Ag^+ and MnO_2, the intensity is enhanced more clearly. These suggest that both MnO_2 and Ag^+ make important roles in the oxidation of OPD, and the sensitivity for detection of Ag^+ can be improved in the presence of MnO_2.

Fluorescence experiment was further applied for proving the mechanism (Fig. 3f). After OPD incubated with MnO_2 nanosheets, the largest fluorescence intensity appeared (a). When GSH incubated with MnO_2 nanosheets prior to addition of OPD (b), the intensity reduced. However, when OPD incubated with MnO_2 nanosheets prior to the addition of GSH (c), there was almost no change in fluorescence intensity compared with MnO_2-OPD. It may suggest that GSH interacts with MnO_2 not OPD. GSH was mixed with Ag^+ firstly, and then the mixed solution incubated with MnO_2 nanosheets prior to the addition of OPD (d), the intensity was enhanced. However, GSH was mixed with MnO_2 and then added Ag^+, finally added OPD (e), the fluorescence intensity is almost the same as the case of (b). These results suggest that the mechanism is based on the redox reaction of MnO_2 and GSH, which affects the oxidase property of MnO_2. However, the addition of Ag^+ will form a complex with GSH and Ag^+ also can oxidize OPD to DAP, leading to the fluorescence and absorbance intensity enhanced.

Optimization of assay conditions

To obtain the optimal experimental conditions, the pH value, temperature, time and concentrations of OPD, GSH and MnO_2 nanosheets were investigated. pH is a crucial detection condition, the optimal conditions was obtained when the pH

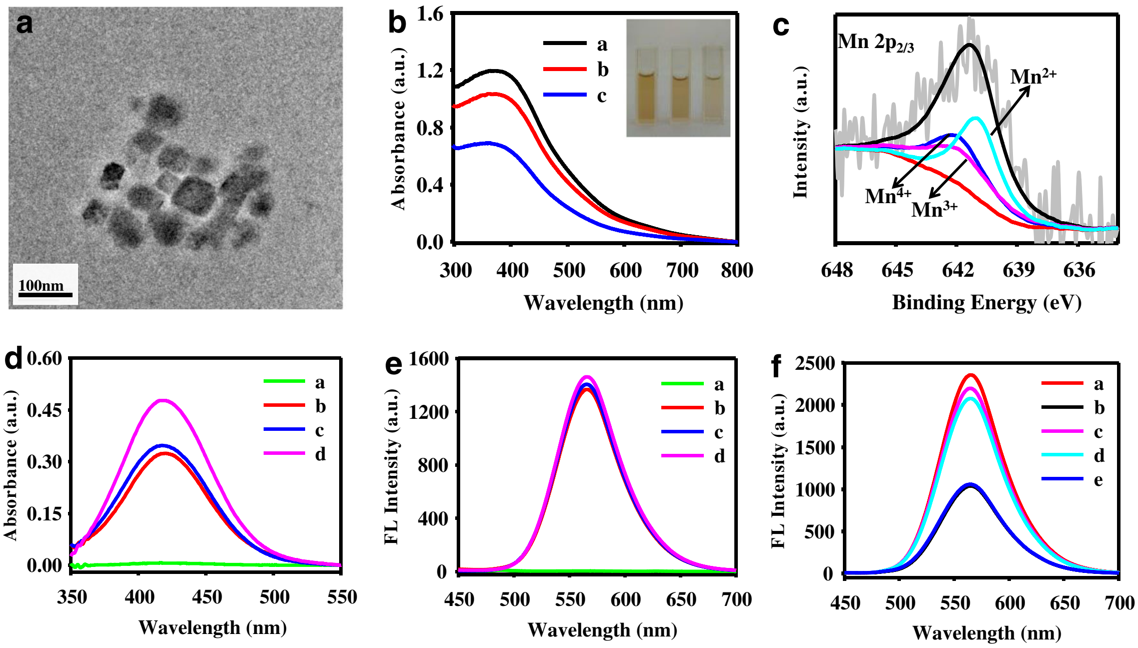

Fig. 3 **a** TEM image of MnO_2 in the presence of GSH. **b** UV-vis absorption spectrum of MnO_2 nanosheets solution in the absence of GSH (a) and in the presence of GSH with concentrations of 10 μM (b) and 50 μM (c), inset shows the photograph of corresponding solution. **c** Deconvoluted Mn $2p_{3/2}$ spectra of MnO_2 nanosheets after reduction by GSH. Absorbance (**d**) and Fluorescence emission (**e**) of OPD (a), OPD incubated with Ag^+ (b) and MnO_2 (c), and OPD incubated with the mixture of MnO_2 and Ag^+ (d). **f** Fluorescence emission spectrum of OPD incubated with MnO_2 nanosheets (a), GSH incubated with MnO_2 nanosheets prior to addition of OPD (b), OPD incubated with MnO_2 nanosheets prior to addition of GSH (c), GSH was mixed with Ag^+ firstly, and then the mixed solution incubated with MnO_2 nanosheets prior to addition of OPD (d), GSH incubated with MnO_2 nanosheets prior to addition of Ag^+, finally OPD was added (e)

value was 7.0 (Fig. S2A, S3A). Reaction temperature influences the reaction speed and stability of reactions, which is also an important for detection. As shown in Fig. S2B and S3B, 60 °C is the optimal reaction temperature. Reaction time also affects the fluorescence intensity, it can be seen that 40 min is the most suitable time for the assay (Fig. S2C, S3C). The concentrations of OPD, MnO_2 nanosheets and GSH are the essential factors in the system, the optimal conditions were obtained when the concentrations of OPD, MnO_2 nanosheets and GSH were 300 μM, 20 μM (Fig. S2E, S3E), 10 μM (Fig. S3F), respectively.

Colorimetric detection of GSH and Ag^+

Under the optimized conditions, the detection of GSH and Ag^+ was firstly conducted based on the MnO_2-OPD using the colorimetric method. In Fig. 4a, it can be seen that the absorbance intensity is decreased linearly with the concentrations of GSH and the linear relationship can be expressed as $A_0 - A = 0.0016$ [GSH] + 0.001 and $A_0 - A = 0.0003$ [GSH] + 0.0266 in the range of 1.0-20 μM ($R^2 = 0.9914$) and 20-80 μM ($R^2 = 0.9916$), where A_0 and A represent the intensity of MnO_2-OPD without or with GSH, respectively. The detection limit of GSH is 0.94 μM ($S/N = 3$) (Fig. 4b). As shown in Fig. 4c, the absorbance intensity is gradually increased with the concentration of Ag^+. As is exhibited in Fig. 4d, the change of absorbance intensity is closely related to Ag^+ concentration and it displays good linear relationship as $A - A_0 = 0.0026\ [Ag^+] - 0.0288$ in the range of 10–70 μM ($R^2 = 0.9907$), where A_0 and A represent the absorbance intensity of MnO_2-OPD and GSH without or with Ag^+, respectively. And the detection limit is 1.15 μM ($S/N = 3$). Therefore, the platform is suitable for detecting GSH and Ag^+ based on the colorimetric method using MnO_2-OPD.

Fluorometric detection of GSH and Ag^+

Owing to the fluorescence method is more sensitive in the detection, the quantify of GSH and Ag^+ was also performed. Different concentration of GSH was added in the MnO_2 solution and then OPD was added at optimal assay conditions. In Fig. 5a, it can be observed that the fluorescence signals at 565 nm are sensitive to GSH, and simultaneously, the fluorescence intensity gradually decreases as the concentrations of GSH increasing. The fluorescence signal linearly decreases in the range from 0.5 to 10 μM. As a result, the linear relationship can be described as $F_0 - F = 45.905[GSH] - 1.893$ with the coefficient of $R^2 = 0.9923$ (Fig. 5b), where F_0 and F represent the FL intensities of MnO_2-OPD in the absence or presence of GSH, respectively. and the detection limit is 62 nM ($S/N = 3$). Similarly, as shown in Fig. 5c, the fluorescence intensity

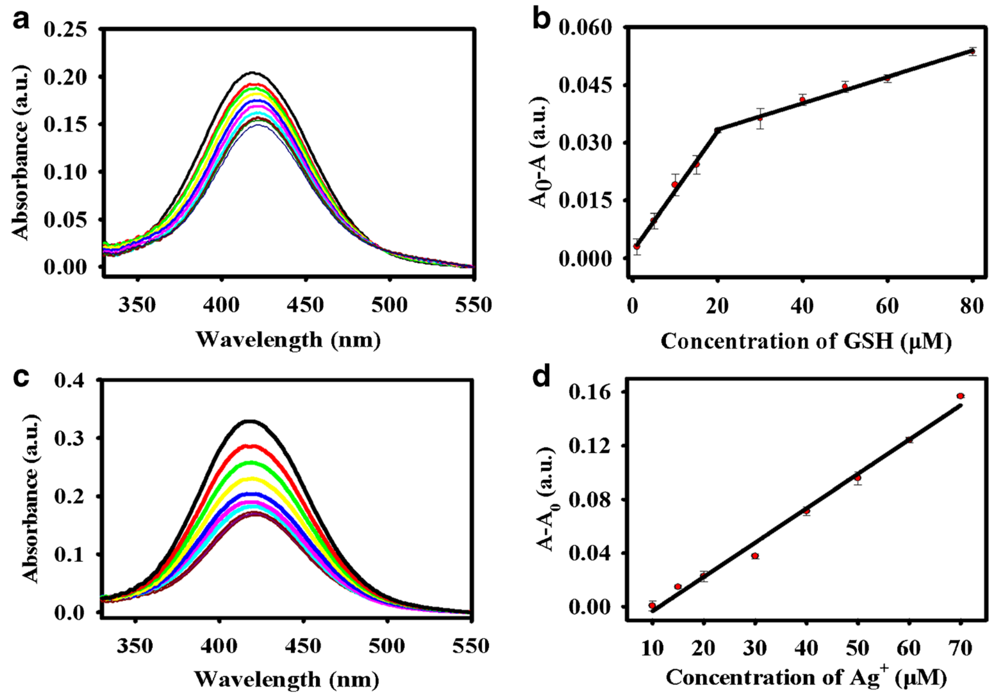

Fig. 4 **a** UV-vis spectra of different concentrations of GSH (0.0, 1.0, 5.0, 10.0, 15.0, 20.0, 30.0, 40.0, 50.0, 60.0, 80.0 μM) incubated with MnO_2 nanosheets prior to addition of OPD. **b** Linear relationship between ($A_0 - A$) and different concentration of GSH (1.0, 5.0, 10.0, 15.0, 20.0, 30.0, 40.0, 50.0, 60.0, 80.0 μM), where A_0 and A represent the intensity of MnO_2-OPD without or with GSH. **c** UV-vis spectra of GSH and different concentrations of Ag^+ (0.0, 10.0, 15.0, 20.0, 30.0, 40.0, 50.0, 60.0, 70.0 μM) incubated with MnO_2 nanosheets and prior to addition OPD. **d** Linear relationship between ($A_0 - A$) and different concentration of Ag^+ (10.0, 15.0, 20.0, 30.0, 40.0, 50.0, 60.0, 70.0 μM), where A_0 and A represent the absorbance intensity of MnO_2-OPD-GSH without or with Ag^+. Inset shows the photograph of corresponding solution

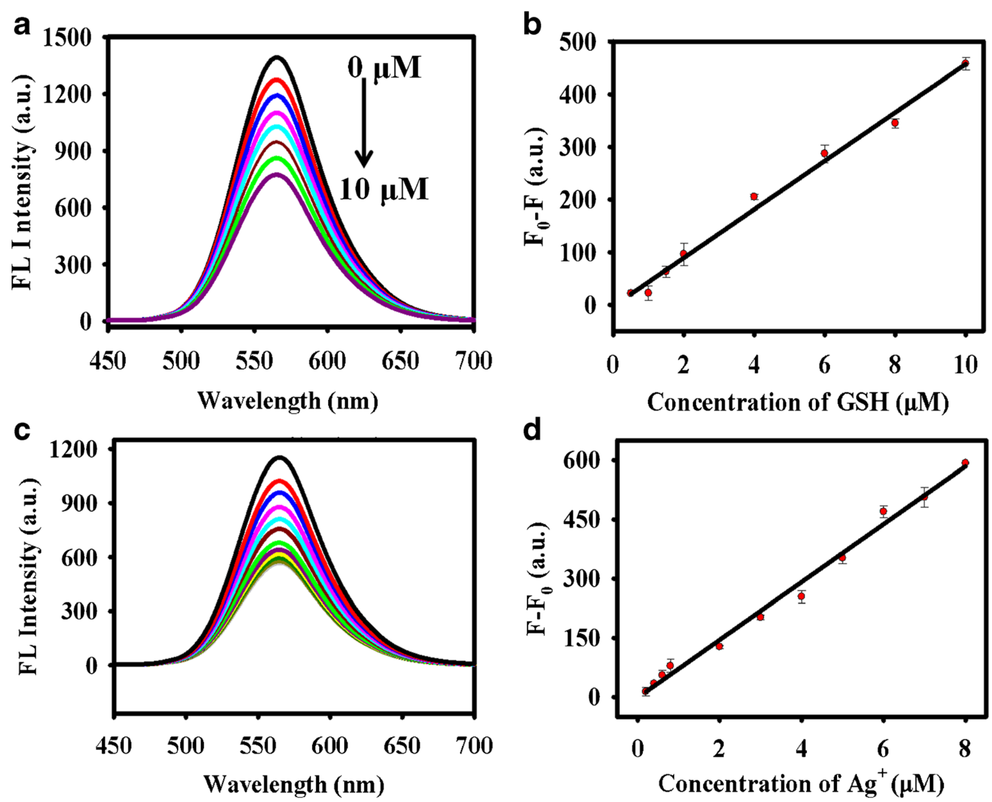

Fig. 5 **a** Fluorescence emission spectrum of GSH with different concentrations (0.0, 0.5, 1.0, 1.5, 2.0, 4.0, 6.0, 8.0, 10.0 μM) incubated with MnO_2 nanosheets prior to addition of OPD. **b** Linear relationship between ($F_0 - F$) and different concentrations of GSH (0.5, 1.0, 1.5, 2.0, 4.0, 6.0, 8.0, 10.0 μM), where F_0 and F represent the FL intensity of MnO_2-OPD without or with GSH. **c** Fluorescence emission spectrum of GSH and different concentrations of Ag^+ (0.0, 0.2, 0.4, 0.6, 0.8, 2.0, 3.0, 4.0, 5.0, 6.0, 7.0, 8.0 μM) incubated with MnO_2 nanosheets and prior to addition of OPD. **d** Linear relationship between ($F - F_0$) and the concentration of Ag^+ (0.2, 0.4, 0.6, 0.8, 2.0, 3.0, 4.0, 5.0, 6.0, 7.0, 8.0 μM), where F_0 and F represent the FL intensity of MnO_2-OPD-GSH without or with Ag^+

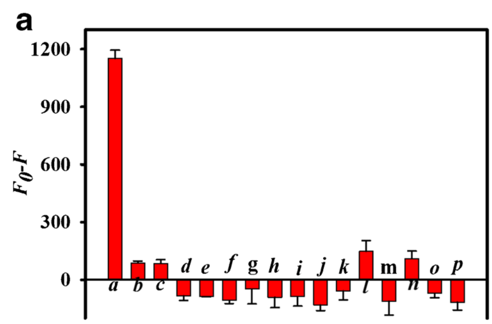

Fig. 6 **a** Selectivity of GSH over potential interferences. The concentrations of GSH (a) was 10 μM, Cys (b) and AA (c) were 1 μM, the concentrations of NaCl (d), KCl (e), $CaCl_2$ (f), $MnCl_2$ (g), $MgSO_4$ (h), Gly (i), Gln (j), His (k), Lys (l), Glu (m), Tyr (n), Ser (o), Ala (p) were 100 μM. **b** Selectivity of the MnO_2-OPD-GSH toward Ag^+, the concentrations of Ag^+ (a) was 10 μM, concentrations of Mn^{2+} (b), Mg^{2+} (c), Hg^{2+} (d), Al^{3+} (e), Ca^{2+} (f), Cd^{2+} (g), Ni^{2+} (h), Zn^{2+} (i), Cu^{2+} (j), Fe^{2+} (n), Fe^{3+} (o), Cr^{3+} (p), Pb^{2+} (q) were 100 μM, concentrations of Na^+ (k), K^+ (l), Co^{2+} (m) was 50 μM, and the solution of Cu^{2+} was added EDTA as mask regent. All experiments were performed in pH 7.0 and the error bar represents the standard deviation for three determinations

is increased with the concentration of Ag^+, the linear relationship is $F - F_0 = 72.907[Ag^+] - 0.9923$ with the coefficient of $R^2 = 0.9905$ (Fig. 5d), where F_0 and F represent the FL intensities of MnO_2-OPD-GSH without or with Ag^+, respectively. The detection limit is as low as 70 nM (S/N = 3). These consequences demonstrate that the MnO_2-based platform can be applied for GSH and Ag^+ detection with good sensitivity. The comparison of the performance of this platform with other reported methods for GSH and Ag^+ are summarized in Table S1. It can be concluded that the detection limit is lower than many other methods. And most of the reports only use single signal or only detecting one component, which is not thoroughly than the dual-readout for multi-components detection.

Table 1 The determination of GSH and Ag^+ in real samples

Sample	Detection objects	Method	Added (μM)	Detected (μM)	Recovery (%) n = 3	RSD (%) n = 3
Human serum samples	GSH	Colorimetric	0.0	–	–	–
			10.0	10.8	108.0	1.2
			50.0	48.9	97.8	0.9
		Fluorescence	0.0	3.3	–	–
			2.0	5.2	95.0	1.8
			6.0	9.5	103.3	2.0
	Ag^+	Colorimetric	0.0	–	–	–
			40.0	37.0	92.5	1.5
			60.0	54.7	91.2	0.7
		Fluorescence	0.0	–	–	–
			2.0	2.2	110.0	1.6
			6.0	6.1	101.6	2.4
Tap water	Ag^+	Colorimetric	0.0	–	–	–
			40.0	43.8	109.5	0.8
			60.0	59.2	98.7	2.5
		Fluorescence	0.0	–	–	–
			2.0	1.81	90.5	2.3
			6.0	5.68	94.7	0.2
River water	Ag^+	Colorimetric	0.0	–	–	–
			40.0	39.9	99.8	1.9
			60.0	54.2	90.3	2.2
		Fluorescence	0.0	–	–	–
			2.0	1.87	93.5	0.9
			6.0	6.79	113.2	1.6

Analytical performance of the method

In order to prove the platform has good selectivity for GSH, some possible interfering molecules including Gly, Gln, His, Lys, Glu, Tyr, Ser, Ala, NaCl, KCl, $CaCl_2$, $MnCl_2$, $MgSO_4$ etc. with the concentration of 100 μM were chosen for study under the same conditions (Fig. 6a) by fluorescence assay because it is more sensitive than colorimetric method. However, large amount of AA and Cys will interfere the detection of GSH owing to its reduction properties which is similar to GSH [32–34]. To this end, decreasing the concentration of AA and Cys to 1 μM can eliminate interference since their biological concentration is much lower than GSH. And it is unlikely to cause significant effect on GSH detection in biological systems [1]. It indicated that the platform could selectively distinguish GSH from other species.

In order to explore the potential application of Ag^+ in real samples, we investigated the stability under various ions including Mn^{2+}, Mg^{2+}, Hg^{2+}, Al^{3+}, Ca^{2+}, Cu^{2+} etc. with the concentration of 100 μM, Na^+, K^+, Co^{2+} with the concentration of 50 μM (Fig. 6b). In the system, Cu^{2+} will cause some interference to the detection of GSH, thus EDTA was chose as a masking agent because it could form more stable complexes with Cu^{2+} [2]. Therefore, the platform based on MnO_2 can be used for selectively detection of Ag^+.

The method exhibits good selectivity toward GSH and Ag^+. In order to evaluate the practical performance, human serum samples and water samples were detected (Table 1) using the standard addition method. The recoveries are observed in the range of 90.3–113.2%, further indicating the reliability of this method.

Conclusions

A fluorometric/colorimetric strategy for sensitive and selective determination of GSH and Ag^+ based on the MnO_2-OPD nanoplatform was constructed via the damage-protection strategy. The dual-readout detection for GSH and Ag^+ exhibits good performance with low detection limits and wide linear ranges. The detection mechanism is based on enzymatic properties of MnO_2 nanosheets, which can catalyze the oxidation of OPD into DAP with fluorescence and colorimetric signal change. While upon GSH introduction, the MnO_2 nanosheets can be rapidly reduced to Mn^{2+}, which affect its enzymatic properties and result in decrease in fluorescence and absorbance intensity of the system. However, when Ag^+ is added, it can form a complex with GSH, thus prevent the destruction of MnO_2 nanosheets. And Ag^+ can catalyze OPD, thus enhancing the fluorescence and absorbance intensity. The efficient preparation of MnO_2 nanosheets, the novel detection mechanism, the excellent applicability in human serum samples and water samples, demonstrate the potential application of MnO_2 nanosheets in clinical diagnosis even early diagnosis of cancer and targeted drugs releasing systems.

Acknowledgments This work was supported by the National Natural Science Foundation of China (21645008, 21305042), Scientific Research Fund of Hunan Provincial Education Department (18A010, 17C0947), Science and Technology Department (14JJ4030), the construct program of the key discipline in Hunan province and the Aid Program for Science and Technology Innovative Research Team in Higher Educational Institutions of Hunan Province.

Compliance with ethical standards The author(s) declare that they have no competing interests.

References

1. Liu J, Meng L, Fei Z, Dyson PJ, Jing X, Liu X (2017) MnO_2 nanosheets as an artificial enzyme to mimic oxidase for rapid and sensitive detection of glutathione. Biosens Bioelectron 90:69–74
2. He L, Lu Y, Wang F, Jing W, Chen Y, Liu Y (2018) Colorimetric sensing of silver ions based on glutathione-mediated MnO_2 nanosheets. Sensors Actuators B Chem 254:468–474
3. Currie LA (1968) Limits for qualitative detection and quantitative determination. Application to radiochemistry. Anal Chem 40:586–593
4. Fang A, Chen H, Li H, Liu M, Zhang Y, Yao S (2017) Glutathione regulation-based dual-functional upconversion sensing-platform for acetylcholinesterase activity and cadmium ions. Biosens Bioelectron 87:545–551
5. Shen R, Yang J, Luo H, Wang B, Jiang Y (2017) A sensitive fluorescent probe for cysteine and Cu^{2+} based on 1,8-naphthalimide derivatives and its application in living cells imaging. Tetrahedron 73:373–377
6. Li Z, Wang Y, Ni Y (2015) A rapid and label-free dual detection of hg (II) and cysteine with the use of fluorescence switching of graphene quantum dots. Sensors Actuators B Chem 207:490–497
7. Guo S, Liu G, Fan C, Pu S (2018) A new diarylethene-derived probe for colorimetric sensing of cu(II) and fluorometric sensing of cu(II) and Zn(II): Photochromism and high selectivity. Sensors Actuators B Chem 266:603–613
8. Sheng J, Jiang X, Wang L, Yang M, Liu Y-N (2018) Biomimetic mineralization guided one-pot preparation of gold clusters anchored two-dimensional MnO_2 Nanosheets for fluorometric/magnetic bimodal sensing. Anal Chem 90:2926–2932
9. Zhou Y, Ma Z (2017) Fluorescent and colorimetric dual detection of mercury (II) by H_2O_2 oxidation of o-phenylenediamine using Pt nanoparticles as the catalyst. Sensors Actuators B Chem 249:53–58
10. Zhu X, Li J, He H, Huang M, Zhang X, Wang S (2015) Application of nanomaterials in the bioanalytical detection of disease-related genes. Biosens Bioelectron 74:113–133
11. Xiong C, Zhang T, Kong W, Zhang Z, Qu H, Chen W, Wangn Y, Luo L, Zheng L (2018) ZIF-67 derived porous Co_3O_4 hollow nanopolyhedron functionalized solution-gated graphene transistors for simultaneous detection of glucose and uric acid in tears. Biosens Bioelectron 101:21–28
12. Hu S, Zhu L, Lam CW (2019) Fluorometric determination of the activity of inorganic pyrophosphatase and its inhibitors by exploiting the peroxidase mimicking properties of a two-dimensional metal organic framework. Microchim Acta 186:190
13. Zhang Q, Wang F, Zhang H, Zhang Y, Liu M, Liu Y (2018) Universal Ti_3C_2 MXenes based self-standard ratiometric

fluorescence resonance energy transfer platform for highly sensitive detection of exosomes. Anal Chem 90:12737–12744
14. Li L, Wang C, Liu K (2015) Hexagonal cobalt oxyhydroxide–carbon dots hybridized surface: high sensitive fluorescence turn-on probe for monitoring of ascorbic acid in rat brain following brain ischemia. Anal Chem 87:3404–3411
15. Ganganboina AB, Doong RA (2018) The biomimic oxidase activity of layered V_2O_5 nanozyme for rapid and sensitive nanomolar detection of glutathione. Sensors Actuators B Chem 273:1179–1186
16. Wei W, Cui X, Chen W, Ivey DG (2011) Manganese oxide-based materials as electrochemical supercapacitor electrodes. Chem Soc Rev 40:1697–1721
17. Liu Z, Xu K, Sun H, Yin S (2015) One-step synthesis of single-layer MnO_2 nanosheets with multi-role sodium dodecyl sulfate for high-performance pseudocapacitors. Small 11:2182–2191
18. Xiao T, Sun J, Zhao J, Wang S, Liu G, Yang X (2018) FRET effect between fluorescent polydopamine nanoparticles and MnO_2 nanosheets and its application for sensitive sensing of alkaline phosphatase. ACS Appl Mater Interfaces 10:6560–6569
19. Han L, Zhang H, Chen D, Li F (2018) Protein-directed metal oxide nanoflakes with tandem enzyme-like characteristics: colorimetric glucose sensing based on one-pot enzyme-free cascade catalysis. Adv Funct Mater 28:1800018
20. Deng R, Xie X, Vendrell M, Chang Y-T, Liu X (2011) Intracellular glutathione detection using MnO_2-nanosheet-modified upconversion nanoparticles. J Am Chem Soc 133:20168–20171
21. Wang X, Wang D, Guo Y, Yang C, Liu X, Iqbal A, Liu W, Qin W, Yan D, Guo H (2016) Fluorescent glutathione probe based on MnO_2-phenol formaldehyde resin nanocomposite. Biosens Bioelectron 77:299–305
22. Wang Q, Zhang Y, Wang X, Wu Y, Dong C, Shuang S (2019) Dual role of BSA for synthesis of MnO_2 nanoparticles and their mediated fluorescent turn-on probe for glutathione determination and cancer cell recognition. Analyst. https://doi.org/10.1039/c8an02501k
23. Qin J, Zhang L, Yang R (2019) Powder carbonization to synthesize novel carbon dots derived from uric acid for the detection of Ag(I) and glutathione. Spectrochim Acta A Mol Biomol Spectrosc 20: 754–760
24. Xu J, Liu N, Hao C, Han Q, Duan Y, Wu J (2019) A novel fluorescence "on-off-on" peptide-based chemosensor for simultaneous detection of Cu^{2+}, Ag^{+} and S^{2-}. Sensors Actuators B Chem 280:129–137
25. He L, Lu Y, Gao X (2018) Self-cascade system based on cupric oxide nanoparticles as dual-functional enzyme mimics for ultrasensitive detection of silver ions. ACS Sustain Chem Eng 6:12132–12139
26. Ni P, Sun Y, Dai H, Hu J, Jiang S, Wang Y, Li Z (2015) Highly sensitive and selective colorimetric detection of glutathione based on Ag [I] ion-3,3,5,5-tetramethylbenzidine (TMB). Biosens Bioelectron 63:47–52
27. Li F, Liu J, Hu Y, Deng N, He J (2018) An ultrasensitive label-free colorimetric assay for glutathione based on Ag^{+} regulated autocatalytic oxidation of o-phenylenediamine. Talanta 186:330–336
28. Liu X, Wang Q, Zhao H, Zhang L, Su Y, Lv Y (2012) BSA-templated MnO_2 nanoparticles as both peroxidase and oxidase mimics. Analyst 137:4552–4558
29. Ge J, Cai R, Chen X, Wu Q, Zhang L, Jiang Y, Tan W (2019) Facile approach to prepare HSA-templated MnO_2 nanosheets as oxidase mimic for colorimetric detection of glutathione. Talanta 195:40–45
30. Rong S, Zhang P, Yang Y, Zhu L, Wang J, Liu F (2017) MnO_2 framework for instantaneous mineralization of carcinogenic airborne formaldehyde at room temperature. ACS Catal 7:1057–1067
31. Qu Z, Bu Y, Qin Y, Wang Y, Fu Q (2013) The improved reactivity of manganese catalysts by Ag in catalytic oxidation of toluene. Appl Catal B Environ 132:353–362
32. Zeng R, Tang Y, Zhang L, Luo Z, Tang D (2018) Dual-readout aptasensing of antibiotic residues based on gold nanocluster-functionalized MnO_2 nanosheets with target-induced etching reaction. J Mater Chem B 6:8071–8077
33. Na W, Li N, Su X (2018) Enzymatic growth of single-layer MnO_2 nanosheets in situ: application to detect alkaline phosphatase and ascorbic acid in the presence of sulfanilic acid functionalized graphene quantum dots. Sensors Actuators B Chem 274:172–179
34. Zhang L, Zhang J, Chen H, Wang L (2018) Redox luminescence switch based on Mn^{2+}-doped $NaYF_4$:Yb,Er upconversion nanorods. Luminescence 33:138–144